

Gauss-Bonnet scalarization of charged qOS-black holes

Hong Guo^{1*}, Wontae Kim^{2,3†}, and Yun Soo Myung^{3‡}

¹Particle Theory and Cosmology Group, Center for Theoretical Physics of the Universe,
Institute for Basic Science (IBS), Daejeon 34126, Republic of Korea

²Department of Physics, Sogang University, Seoul, 04107, Republic of Korea

³Center for Quantum Spacetime, Sogang University, Seoul 04107, Republic of Korea

Abstract

The Gauss-Bonnet (GB) scalarization for charged quantum Oppenheimer-Snyder (cqOS)-black holes is investigated in the Einstein-Gauss-Bonnet-scalar theory with the nonlinear electrodynamics (NED) term. Here, the scalar coupling function to GB term is given by $f(\phi) = 2\lambda\phi^2$ with a coupling constant λ . Three parameters of mass (M), action parameter (α), and magnetic charge (P) are necessary to describe the cqOS-black hole, and it may become the qOS-black hole when $P = M$. The GB scalarization of cqOS-black holes comes into two cases GB^\pm , depending on the sign of GB term which triggers the different phenomena. For $\alpha = 0$ and $\lambda > 0$, GB^+ scalarization is allowed, while for $\alpha \neq 0$ and $\lambda < 0$, GB^- scalarization appears for a narrow band of $3.5653 \leq \alpha \leq 4.6875$. After discussing the onset GB^- scalarization, we construct scalarized qcOS-black holes which belong to the single branch. The scalar field is nonmonotonic near the horizon while it asymptotes to a finite value at infinity, indicating a distinct scalarization mechanism for negative coupling λ . Stability analysis shows these scalarized black holes are linearly stable under scalar perturbations.

*e-mail address: guohong@ibs.re.kr

†e-mail address: wtkim@sogang.ac.kr

‡e-mail address: ysmyoung@inje.ac.kr

1 Introduction

It is well-known as no-hair theorem that a black hole can be described by three classical parameters of mass, electric charge, and angular momentum in Einstein gravity [1, 2]. Considering a minimally coupled scalar field to gravitational and Maxwell fields with a positive scalar potential, there are no black hole solutions with scalar hair [3]. However, its evasion appeared immediately for a nonminimally coupled scalar to either Gauss-Bonnet (GB) term [4, 5, 6], or Maxwell (M) term with a positive (+) coupling constant [7, 8, 9]. The former case denotes curvature-induced (GB⁺) spontaneous scalarization of Schwarzschild black hole, while the latter represents charged-induced (M⁺) spontaneous scalarization of Reissner-Nordström black hole. In these cases triggered by tachyonic instability, one obtained infinite branches of scalarized black holes from infinite scalar clouds.

For the negative (−) coupling constant, the spin-induced (GB[−]) scalarization of Kerr black holes with mass M and rotation parameter a were studied in the Einstein-Gauss-Bonnet-Scalar (EGBS) theory [10, 11]. Here, an a -bound of $a_c(= 0.5) \leq a \leq 1$ with $M = 1$ was found to describe the condition for onset of GB[−] scalarization [12, 13, 14, 15]. This indicates that GB[−] scalarization is forbidden for the low rotation of $0 < a < a_c$. Furthermore, the condition for spin-induced (M[−]) scalarization of Kerr-Newman black holes was found to be $a_c(= 0.672) \leq a \leq 1$ for mass $M = 1$ and charge $Q = 0.4$ [16] as well as the spin-charge induced scalarization of Kerr-Newman black holes was studied in Einstein-Maxwell-Scalar (EMS) theory [17]. Also, it is notified that the dual coupling concept of curvature and matter-induced scalarization discussed in the EGBMS theory [18].

Recently, the quantum Oppenheimer-Snyder (qOS) black hole was found by studying the qOS gravitational collapse in conjunction with the loop quantum cosmology [19]. An undesirable point to this approach is that an explicit action \mathcal{L}_{qOS} is not known and thus, its energy momentum tensor was used to obtain qOS black hole. Explicitly, the qOS-black hole was obtained by applying the junction conditions but not solving the equations of motion. Various applications of this model were studied by including thermodynamics [20], shadow radius [21], and onset GB[−] scalarization [22]. In addition, quantum parameter-mass induced (GB[−]) scalarization was studied in the EGBS theory [23], showing a deep connection between thermodynamics of qOS-black hole and onset GB[−] scalarization.

However, one could not make a further progress to obtain its scalarized qOS-black holes because of unknowing its action \mathcal{L}_{qOS} . Regarding to appropriate actions for \mathcal{L}_{qOS} , a

candidate was proposed by considering a nonlinear electrodynamics (NED) term. In this case, one found cqOS-black hole solution and the qOS black hole solution may be recovered when imposing $P = M$ which is not the extremal condition [24]. Inspired by this work, we will investigate scalarized cqOS-black holes in the EGBS-NED theory with a scalar coupling $f(\phi)$ to the GB term.

The organization of the present work is as follows. In section 2, we obtain the cqOS-black holes. We briefly mention thermodynamics of the cqOS-black hole described by mass (M) and action parameter (α) with a fixed magnetic charge P . Section 3 is devoted to discussing onset GB⁻ scalarization of cqOS-black holes. Here, one finds that two Davies quantities of heat capacity are not identified with two critical onset parameters for GB⁻ scalarization. This implies that this black hole is not really considered as the qOS black hole. We will obtain scalarized cqOS-black holes through GB⁻ scalarizations in section 4. Section 5 is focused on performing the stability analysis of scalarized cqOS-black holes.

2 cqOS-black holes and its thermodynamics

The EGBS-NED theory is introduced as

$$\mathcal{L}_{\text{EGBS-NED}} = \frac{1}{16\pi} \left[R - 2\partial_\mu\phi\partial^\mu\phi + f(\phi)\mathcal{R}_{\text{GB}}^2 + \mathcal{L}_{\text{NED}} \right] \quad (1)$$

where $\mathcal{R}_{\text{GB}}^2$ denotes the GB term of $R^2 - 4R_{\mu\nu}R^{\mu\nu} + R_{\mu\nu\rho\sigma}R^{\mu\nu\rho\sigma}$ and the NED term is given by $\mathcal{L}_{\text{NED}} = -2\xi(\mathcal{F})^{\frac{3}{2}}$ with $\mathcal{F} = F_{\mu\nu}F^{\mu\nu}$. To explore GB[±] scalarizations, a quadratic scalar coupling $f(\phi) = 2\lambda\phi^2$ is chosen with positive/negative coupling constant λ .

We obtain the Einstein equation from the EGBS-NED theory

$$G_{\mu\nu} = 2\partial_\mu\phi\partial_\nu\phi - (\partial\phi)^2g_{\mu\nu} + \Gamma_{\mu\nu} + T_{\mu\nu}^{\text{NED}}, \quad (2)$$

where the GB-scalar coupling term $\Gamma_{\mu\nu}$ takes the form with $\Psi_\mu = f'(\phi)\partial_\mu\phi$

$$\begin{aligned} \Gamma_{\mu\nu} &= 2R\nabla_{(\mu}\Psi_{\nu)} + 4\nabla^\alpha\Psi_\alpha G_{\mu\nu} - 8R_{(\mu|\alpha|}\nabla^\alpha\Psi_{\nu)} \\ &+ 4R^{\alpha\beta}\nabla_\alpha\Psi_\beta g_{\mu\nu} - 4R^\beta_{\mu\alpha\nu}\nabla^\alpha\Psi_\beta. \end{aligned} \quad (3)$$

In addition, the NED energy-momentum tensor is given by

$$T_{\mu\nu}^{\text{NED}} = 6\xi\sqrt{\mathcal{F}} \left[F_{\mu\lambda}F_\nu^\lambda - \frac{1}{6}\mathcal{F}g_{\mu\nu} \right]. \quad (4)$$

The nonlinear-Maxwell equation is given by $\nabla_\mu(\sqrt{\mathcal{F}}F^{\mu\nu}) = 0$ [24]. Taking into account a magnetic field strength $F_{\theta\varphi} = q \sin\theta$ ($\mathcal{F} = 2q^2/r^4$) and $\xi = 2^{-3/2}3\alpha/P$, Eq.(4) is given by an anisotropic energy-momentum tensor

$$T_\mu^{\text{NED},\nu} = \frac{3\alpha P^2}{r^6} \text{diag}[-1, -1, 2, 2] \equiv \text{diag}[-\rho, p_r, p_\theta, p_\phi]. \quad (5)$$

It satisfies three (null, weak, strong) energy conditions for $\alpha > 0$, except that the dominant energy condition of $\rho \geq |p_i|$ is violated.

On the other hand, the scalar equation indicates

$$\square\phi + \frac{1}{4}f'(\phi)\mathcal{R}_{\text{GB}}^2 = 0. \quad (6)$$

Solving the Einstein equation (2) without scalar ($\phi = 0$), one finds the cqOS-black hole solution

$$ds_{\text{cqOS}}^2 = \bar{g}_{\mu\nu}dx^\mu dx^\nu = -g(r)dt^2 + \frac{dr^2}{g(r)} + r^2 d\Omega_2^2 \quad (7)$$

whose metric function is given by [19]

$$g(r) \equiv 1 - \frac{2\tilde{m}}{r} = 1 - \frac{2M}{r} + \frac{\alpha P^2}{r^4}, \quad (8)$$

where mass function \tilde{m} is defined. From $\tilde{m} = 0$, one may define the bouncing radius

$$r_b(M, \alpha, P) = \left(\frac{\alpha P^2}{2M}\right)^{1/3} \quad (9)$$

which can be also obtained from the junction condition. Choosing $P = M$ leads to the qOS black hole [19], but this fixing seems to be unnatural. This choice has nothing to do with the condition for the extremality. Instead, it suggests the nature of the present model as charged quantum Oppenheimer-Snyder model [24] because its (P) role is similar to α and all expressions pertaining P came out as “ αP^2 ”. It is interesting to note that the electrically charged black hole solution was found for \mathcal{F}^n in the Einstein-NED theory [25].

Let us mention briefly the thermodynamics of cqOS-black hole with Smarr formula by looking for the outer horizon r_+ . Solving $g(r) = 0$, one finds two real and complex solutions

$$r_i(M, \alpha, P), \quad \text{for } i = 4, 3, 2, 1. \quad (10)$$

Here, we note that r_4 is replaced by r_+ and r_3 is denoted by r_- , but $r_{2/1}$ become complex solutions. The extremal black hole and the remnant for $r_+ = r_-$ occur for

$$\alpha_\epsilon(M, P) = \frac{27M^4}{16P^2}, \quad M_{\text{rem}}(\alpha, P) = 2\sqrt{\frac{P\sqrt{\alpha}}{3\sqrt{3}}}, \quad (11)$$

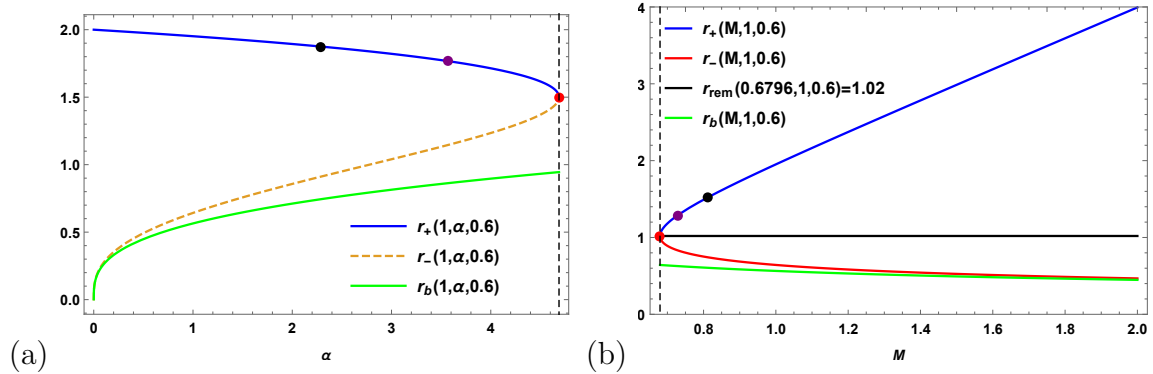


Figure 1: (a) Two outer/inner horizons $r_{\pm}(M = 1, \alpha, P = 0.6)$ are functions of $\alpha \in [0, 4.6875]$. The bouncing radius $r_b(1, \alpha, 0.6)$ as function of α is inside the inner horizon. Here, $r_+(1, \alpha, 0.6)$ involves the Davies point at $[(2.29, 1.88)$, black dot], critical onset point $[(3.5653, 1.7676)$, purple dot], and extremal point $[(4.6875, 1.5)$, red dot]. (b) Two horizons $r_{\pm}(M, \alpha = 1, P = 0.6)$ are functions of $M \in [M_{\text{rem}} = 0.6796, \infty]$, showing the lower mass bound [remnant point at $(0.6796, 1.02)$, red dot]. The black dot represents the Davies point at $(0.81, 1.52)$, while the purple dot denotes the critical onset point at $(0.7277, 1.286)$. The bouncing radius is located inside the inner horizon.

which leads to $\alpha_e = 4.6875$ for $M = 1, P = 0.6$ and $M_{\text{rem}} = 0.6796$ for $\alpha = 1, P = 0.6$. As is shown in Fig. 1(a), there is an upper bound on α (extremal point $\alpha = \alpha_e$ for $M = 1$), while there is a lower bound for the mass of black hole (remnant mass $M = M_{\text{rem}}$ for $\alpha = 1$) but there is no upper bound on the mass [see Fig. 1(b)].

Let us introduce thermodynamics of cqOS-black hole to make its connection to onset GB^- scalarization. We find that black hole mass $m = (\alpha P^2 + r_+^4)/2r_+^3$, the area-law entropy $S = \pi r_+^2$, the Hawking temperature T and the heat capacity C with chemical potential $W_\alpha = P^2/r_+^3$ as

$$T(M, \alpha, P) = \frac{r_+^4(M, \alpha, P) - 3\alpha P^2}{4\pi r_+^5(M, \alpha, P)}, \quad (12)$$

$$C(M, \alpha, P) = - \frac{2\pi r_+^2(M, \alpha, P)[r_+^4(M, \alpha, P) - 3\alpha P^2]}{r_+^4(M, \alpha, P) - 15\alpha P^2}. \quad (13)$$

The first-law of thermodynamics and Smarr formula are satisfied as

$$dm = TdS + W_\alpha d\alpha, \quad m = 2TS + 4W_\alpha \alpha, \quad (14)$$

which indicates that the action parameter α plays the role of a thermodynamic variable,

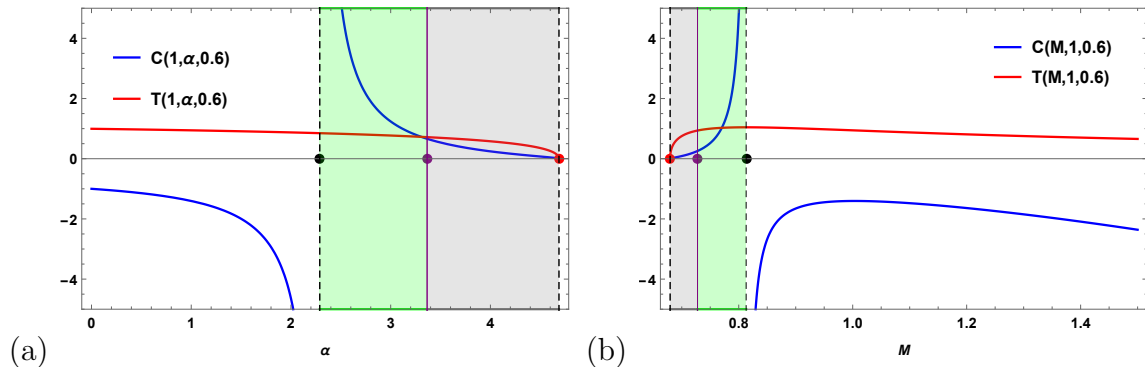


Figure 2: Heat capacity $C(M, \alpha, P)/|C_S(1, 0, 0)|$ with $|C_S(1, 0, 0)| = 25.13$ and temperature $T(M, \alpha, P)/0.04$. (a) Heat capacity $C(M = 1, \alpha, P = 0.6)$ blows up at Davies point ($\alpha_D = 2.29$, \bullet) and it is zero at the extremal point ($\alpha_e = 4.6875$, red dot). The shaded region represents $C \geq 0$ and it is divided at a line ($\alpha = \alpha_c = 3.5653$). (b) Heat capacity $C(M, 1, 0.6)$ blows up at Davies point ($M_D = 0.81$, \bullet). The heat capacity and temperature are zero at the remnant point ($M_{\text{rem}} = 0.6796$, red dot). The shaded region denotes $C \geq 0$, but it is divided at a line ($M = M_c = 0.7277$).

instead of magnetic charge P . Hereafter, we fix $P = 0.6$ for convenience. Considering Eqs. (12) and (13) together with Fig. 2, T and C are zero when their numerators are zero, showing extremal and remnant points, while C blows up when its denominator is zero, leading to the Davies point for a sharp phase transition. We note that two shaded regions represent positive heat capacity ($C \geq 0$). Each shaded region is divided at the line ($\alpha = \alpha_c = 3.5653/M = M_c = 0.7277$) and two gray regions are consistent with the allowed regions for onset GB^- scalarization.

In this case, we define the numerator-zero condition [$nc = 0$] and the condition for denominator-zero [$dc = 0$] of heat capacity C defined as

$$nc(M, \alpha, P) \equiv r_+^4(M, \alpha, P) - 3\alpha P^2 = 0, \quad (15)$$

$$dc(M, \alpha, P) \equiv r_+^4(M, \alpha, P) - 15\alpha P^2 = 0. \quad (16)$$

The former contains the extremal/remnant points ($C \rightarrow 0$, termination), while the latter includes the Davies point ($C \rightarrow \infty$, a sharp phase transition).

3 Onset of GB⁻ scalarization

In this section, we wish to study the onset GB⁻-scalarization of cqOS-black hole by computing critical onset mass M_c and action parameter α_c . For this purpose, we start with the linearized scalar equation: $(\bar{\square} + \lambda \bar{\mathcal{R}}_{\text{GB}}^2)\delta\phi = 0$. Let us introduce a tortoise coordinate defined by $dr_* = dr/g(r)$ and a separation of variables

$$\delta\phi(t, r_*, \theta, \varphi) = \sum_m \sum_{l=|m|}^{\infty} \frac{\psi_{lm}(t, r_*)}{r} Y_{lm}(\theta, \varphi). \quad (17)$$

The linearized $s(l=0, m=0)$ -scalar equation reduces to

$$\frac{\partial^2 \psi_{00}(t, r_*)}{\partial r_*^2} - \frac{\partial^2 \psi_{00}(t, r_*)}{\partial t^2} = V(r)\psi_{00}(t, r_*), \quad (18)$$

where the scalar potential $V(r)$ is given by

$$V(r) = g(r) \left[\frac{2M}{r^3} - \frac{4\alpha P^2}{r^6} + m_{\text{eff}}^2(r) \right] \quad (19)$$

with its effective mass term

$$m_{\text{eff}}^2(r) \equiv -\lambda \bar{\mathcal{R}}_{\text{GB}}^2 = -\frac{48\lambda M^2}{r^6} \left[\frac{3\alpha^2 P^4}{M^2 r^6} - \frac{5\alpha P^2}{Mr^3} + 1 \right]. \quad (20)$$

For $\lambda > 0$ and $\psi_{00}(t, r_*) \sim u(r_*)e^{-i\omega t}$, GB⁺ scalarization of Schwarzschild black hole was found for $\alpha = 0$ [4, 5, 6]. For $\lambda < 0$, one expects to find GB⁻ scalarization with $\alpha \neq 0$. From Fig. 3, it is clear that the mass term $m_{\text{eff}}^2 = -\lambda \bar{\mathcal{R}}_{\text{GB}}^2$ could be negative when $\bar{\mathcal{R}}_{\text{GB}}^2$ is negative for $\alpha_c \leq \alpha \leq \alpha_e$ in the near-extremal region and $M_{\text{rem}} \leq M \leq M_c$ in the near-remnant region with $\lambda < 0$.

Now, we are in a position to find the critical onset parameter α_c and mass M_c , which determine the lower and upper bounds ($\alpha \geq \alpha_c$, $M \leq M_c$) for the onset of GB⁻ scalarization by making use of the Hod's approach [13]. To get the critical onset parameters, it is enough to consider the potential term: $V(r)\psi_{00}(t, r_*) = 0$. The onset of scalarization is defined by critical black hole which denotes the boundary between cqOS- and scalarized cqOS-black holes existing in the limit of $\lambda \rightarrow -\infty$. In this limit, it is characterized by the presence of a degenerate binding potential well whose two turning points merge at the outer horizon of $r = r_+(M, \alpha, P)$ as

$$m_{\text{eff}}^2(r_+)\psi_{00}(t, r_*) = 0. \quad (21)$$

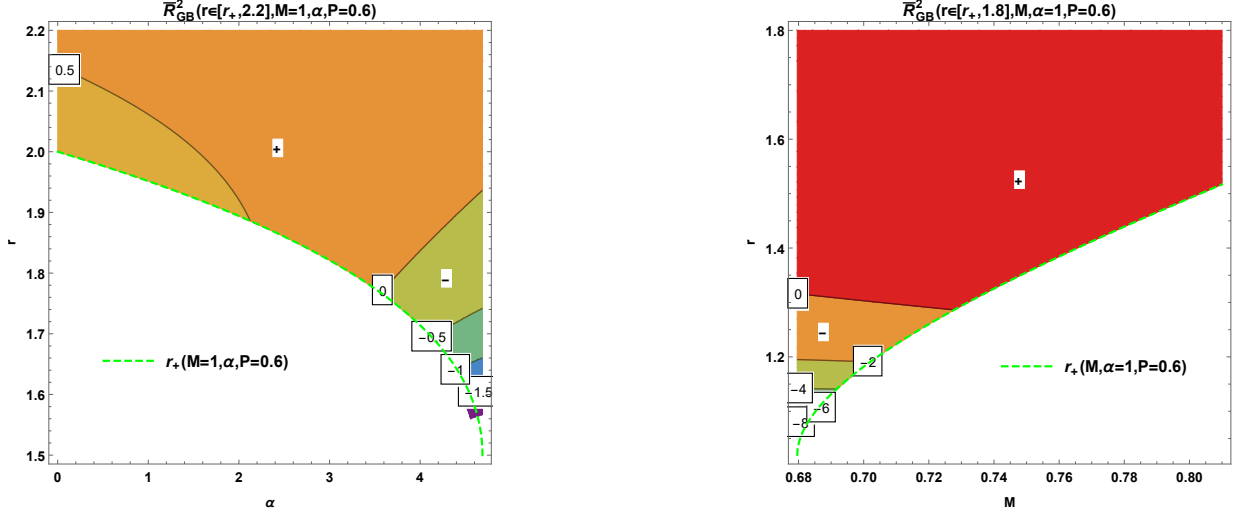


Figure 3: (Left) $\bar{\mathcal{R}}_{\text{GB}}^2(r, M = 1, \alpha, P = 0.6)$ as functions of $r \in [r_+(M = 1, \alpha, P = 0.6), 2.2]$ and $\alpha \in [0, \alpha_e = 4.6875]$ and its zero line is available, starting from $\alpha = \alpha_c (= 3.5653)$ on the horizon. (Right) $\bar{\mathcal{R}}_{\text{GB}}^2(r, M, \alpha = 1, P = 0.6)$ as functions of $r \in [r_+(M, \alpha = 1, P = 0.6), 1.8]$ and $M \in [M_{\text{rem}} = 0.6796, 0.81]$ and its zero line is available, ending at $M = M_c (= 0.7277)$ on the horizon.

From Eq.(21), we find the resonance condition as

$$rc(M, \alpha, P) \equiv \frac{3\alpha^2 P^4}{M^2 r_+^6} - \frac{5\alpha P^2}{M r_+^3} + 1 = 0. \quad (22)$$

The critical onset action parameter and mass are determined by the resonance condition

$$3\tilde{\alpha}^2 - 5\tilde{\alpha} + 1 = 0, \quad \tilde{\alpha} = \frac{\alpha P^2}{M r_+^3}. \quad (23)$$

Solving $\tilde{\alpha} = 0.2324$ for $\alpha = \alpha_c$ with $M_c = 1$ and $P = 0.6$, and for $M = M_c$ with $\alpha_c = 1$ and $P = 0.6$ leads to the critical onset mass and action parameter for GB^- scalarization as

$$(M_c = 1, \alpha_c = 3.5653) \quad \text{and} \quad (M_c = 0.7277, \alpha_c = 1). \quad (24)$$

Fig. 4 shows that $\{dc(M_D, \alpha_D, 0.6) = 0\} \neq \{rc(M_c, \alpha_c, 0.6) = 0\}$, implying that Davies curve cannot be consistent with critical onset (resonance) curve. Observing Fig. 2, $\alpha = \alpha_c$ is regarded as the lower bound for GB^- scalarization ($\alpha_c \leq \alpha \leq \alpha_e$, $C > 0$), while $M = M_c$ is considered as the upper bound for GB^- scalarization ($M_{\text{rem}} \leq M \leq M_c$, $C > 0$). It is worth noting that the presence of such restrictions may lead to the single branch of scalarized cqOS-black holes.

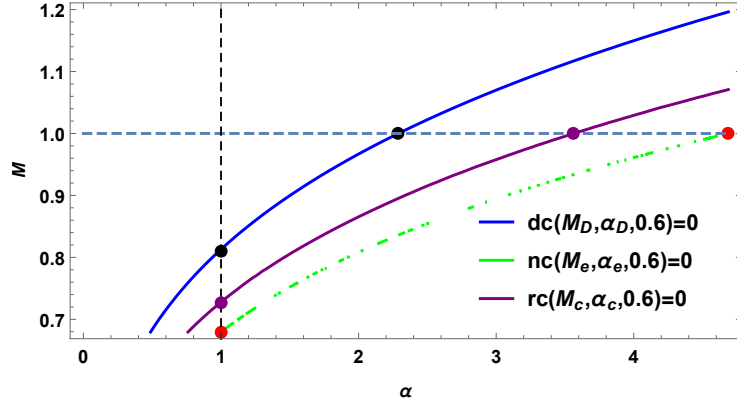


Figure 4: Three different curves for $nc(M_e, \alpha_e, 0.6) = 0$, $dc(M_D, \alpha_D, 0.6) = 0$, and $rc(M_c, \alpha_c, 0.6) = 0$ for $M \in [0.6796, 1.2]$ and $\alpha \in [0, 4.6875]$, including extremal/remnant points (red dot), two Davies points (black dot), and two resonance points (purple dot) for $M = 1$ and $\alpha = 1$.

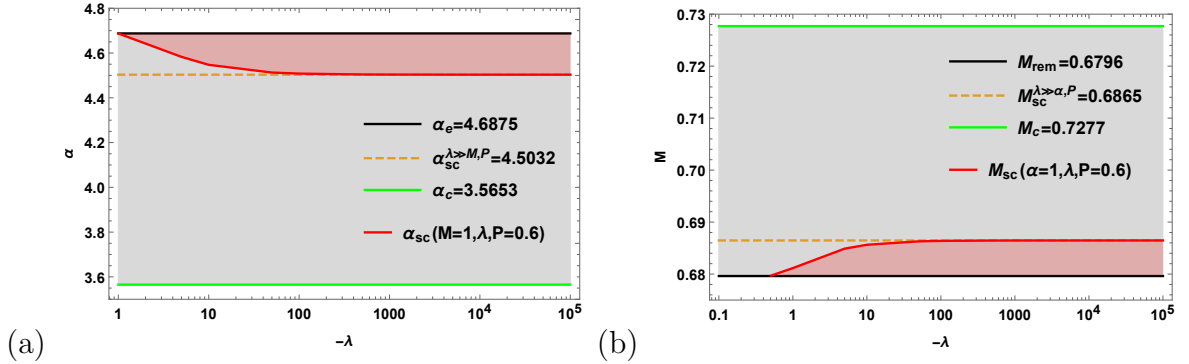


Figure 5: (a) Sufficient condition of $\alpha_{sc}(M = 1, \lambda, P = 0.6)$ with the critical onset parameter $\alpha = \alpha_c$ as the lower bound. A dashed line denotes the sufficient condition $\alpha = \alpha_{sc}^{-\lambda \gg M, P}$. A top line denotes the extremal point at $\alpha = \alpha_e$ as the upper bound. (b) Graph for $M_{sc}(\alpha = 1, \lambda, P = 0.6)$ with the critical onset mass $M = M_c$ as the upper bound and the sufficient condition $M = M_{sc}^{-\lambda \gg \alpha, P}$. A bottom line represents the remnant point at $M = M_{rem}$ as the lower bound.

On the other hand, the sufficient condition for the instability can be obtained by imposing $\int_{r_+}^{\infty} V(r)dr/g(r) < 0$ [26]. For $-\lambda \gg M, \alpha, P$, this condition can reduce to

$$\int_{r_+}^{\infty} m_{\text{eff}}^2(r)dr \equiv I < 0, \quad (25)$$

which leads to

$$I = \frac{6(120\alpha^2 P^4 - 275\alpha P^2 M r_+^3 + 88M^2 r_+^6)}{55r_+^{11}} < 0. \quad (26)$$

We solve $I = 0$ to find two sufficient conditions: $\alpha_{sc}^{-\lambda \gg M, P} = 4.5032$ for $M = 1$, $M_{sc}^{-\lambda \gg \alpha, P} = 0.6865$ for $\alpha = 1$.

To find $\alpha_{sc}(M = 1, \lambda, P = 0.6)$ and $M_{sc}(\alpha = 1, \lambda, P = 0.6)$, we analyze the condition of $\int_{r_+}^{\infty} V(r)dr/g(r) < 0$ numerically for a given λ . As is depicted in Fig. 5, we find that $\alpha_{sc}(1, \lambda, 0.6)$ is a decreasing function, connecting between α_e and $\alpha_{sc}^{-\lambda \gg M, P}$, while $M_{sc}(1, \lambda, 0.6)$ is an increasing function, connecting between M_{rem} and $M_{sc}^{-\lambda \gg \alpha, P}$. We note that two red-shaded regions represent sufficiently unstable region for GB^- scalarization.

Finally, to obtain the threshold of instability [$\alpha_{th}(M = 1, \lambda, P = 0.6)$ and $M_{th}(\alpha = 1, \lambda, P = 0.6)$] which can connect from (α_c, M_{min}) to (α_e, M_c) , one has to solve Eq.(18) to find its time-dependent behaviors by utilizing the fourth-order Runge-Kutta method for time evolution and considering an initial Gaussian wave-packet of $\psi_{0,0}(0, r_*) = e^{-(r_* - r_*^c)^2/\lambda}$ [16, 17, 22]. For a given λ , its time-independent behavior determines the threshold of instability [$\alpha_{th}(M = 1, \lambda, P = 0.6)$ and $M_{th}(\alpha = 1, \lambda, P = 0.6)$] for GB^- scalarization. However, we realize that this task will amount to the other project.

4 Scalarized charged black holes

Instead of finding the thresholds of instability $\alpha_{th}(1, \lambda, 0.6)$, we directly obtain scalarized cqOS-black holes by solving the full equations. For this purpose, we adopt the following metric and field ansatz [4, 27]:

$$ds^2 = -A(r)dt^2 + \frac{dr^2}{B(r)} + r^2(d\theta^2 + \sin^2\theta d\phi^2), \quad \phi = \psi(r), \quad A = A_\varphi. \quad (27)$$

Substituting the gauge field ansatz into the Maxwell equation yields the magnetic potential $A_\varphi = -P \cos\theta$, which in turn determines $F_{\theta\varphi} = P \sin\theta$ and $\mathcal{F} = 2P^2/r^4$. This implies that an approximate solution for A_φ is unnecessary and thus, the nonlinear-Maxwell equation is solved exactly in this case. Then, two equations (2) and (6) reduce to the forms

$$-\frac{6\alpha P^2}{r^4} + \frac{rB'}{2} + \left(\frac{r^2B}{2} - 8\lambda rB^2\psi\psi'\right)\frac{A''}{A} + \left(-\frac{r^2B}{4} + 4\lambda rB^2\psi\psi'\right)\frac{A'^2}{A^2} + \left(\frac{rB}{2} + B'\left(\frac{r^2}{4} - 12\lambda rB\psi\psi'\right) - 8\lambda rB^2(\psi'^2 + \psi\psi'')\right)\frac{A'}{A} + r^2B\psi'^2 = 0, \quad (28)$$

$$1 - \frac{3\alpha P^2}{r^4} - B'(r + 8\lambda\psi\psi') - B\left(1 + (r^2 + 16\lambda)\psi'^2 - 8\lambda\psi(3B'\psi' - 2\psi'')\right) + 16\lambda B^2(\psi'^2 + \psi\psi'') = 0, \quad (29)$$

$$\psi'' + \frac{1}{2}\left(\frac{4}{r} + \frac{A'}{A} + \frac{B'}{B}\right)\psi' + \frac{2\lambda\psi}{r^2A^2B}\left(A'[-(-1+B)BA' + A(-1+3B)B'] + 2A(-1+B)BA''\right) = 0. \quad (30)$$

Considering the existence of outer horizon located at $r = r_+$, the near-horizon solution to Eqs. (28)-(30) can be expressed as [6]

$$A(r) = A_1(r - r_+) + A_2(r - r_+)^2 \dots, \quad (31)$$

$$B(r) = B_1(r - r_+) + B_2(r - r_+)^2 + \dots, \quad (32)$$

$$\psi(r) = \psi_0 + \psi_1(r - r_+) + \dots. \quad (33)$$

Here, the constant scalar $\psi_0 = \psi(r_+)$ at the horizon can be determined when matching with an asymptotically flat solution in the far-region

$$\{A, B\} = 1 + \sum_n \frac{\{p_n, q_n\}}{r^n}, \quad \psi = \psi_\infty + \sum_n \frac{d_n}{r^n} \quad (34)$$

with coefficients of p_n , q_n , and d_n to be determined. A choice of ψ_∞ depends on the sign of coupling constant λ .

4.1 GB⁺ scalarization with $\alpha = 0$ and $\lambda > 0$

For $\alpha = 0$ and $\lambda > 0$, this model reduces to carrying out the GB⁺ scalarization for Schwarzschild black hole in the ESGB theory. With the positive coupling parameter λ , one may find the usual GB⁺ scalarization of Schwarzschild black hole, giving infinite branches of scalarized black holes from infinite scalar clouds [28]. Here, its branches are determined by $\frac{r_+}{2\sqrt{\lambda_n}} = 1.174(n = 0)$, $0.453(n = 1)$, $0.280(n = 2)$, $0.202(n = 3)$. For the fundamental ($n = 0$) branch, its starting point is given by $\lambda_0 = 1.0188$ for $r_+ = 2.37$. Hence, its scalarized black hole solutions are allowed for $\lambda \geq \lambda_0$ in the fundamental branch.

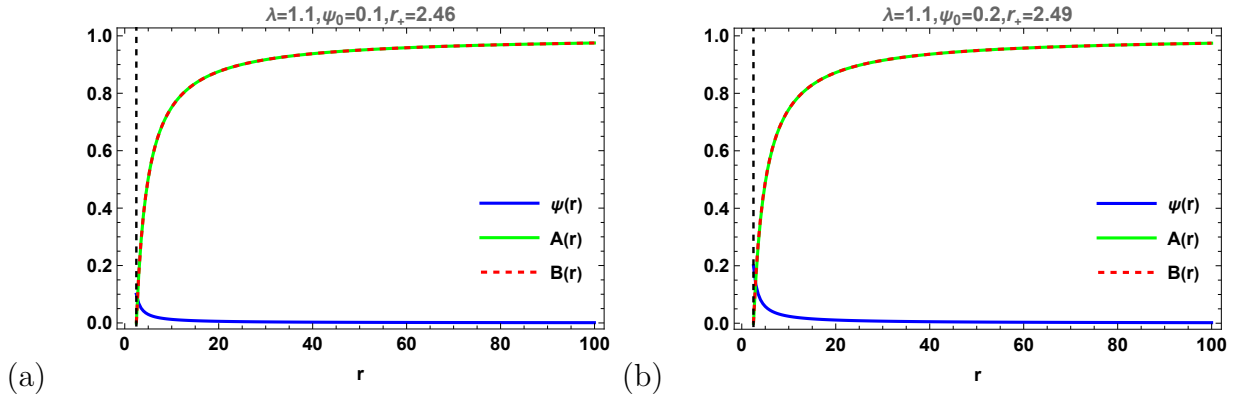


Figure 6: Scalarized black holes obtained from GB^+ scalarization with $P = 0, \alpha = 0, \lambda = 1.1, r_+ = 2.37$ for (a) $\psi_0 = 0.1$ and (b) $\psi_0 = 0.2$ in the fundamental branch.

To obtain the scalarized black hole solution in the $n = 0$ branch, we wish to set $\psi_\infty = 0$ and $A(\infty) = B(\infty)$ as the shooting condition to solve Eqs. (28)-(30) numerically. For $\lambda = 1.1 > \lambda_0$, we select $\psi_0 = 0.1$ and 0.2 to represent the radial profiles for metric functions and scalar field in Fig. 6. It is observed that the scalar field decays monotonically and rapidly approaches zero as r increases. Meanwhile, the metric functions $A(r)$ and $B(r)$ are zero at the horizon, then increase monotonically, approach 1 at infinity, and nearly coincide with each other throughout radial space. There is no sizable difference between $\psi_0 = 0.1$ and $\psi_0 = 0.2$.

4.2 GB^- scalarization with $\alpha \neq 0$ and $\lambda < 0$

To find scalarized cQOS-black holes in the single branch, we choose $P = 0.6$ and $\alpha = 4.6$ which belongs to $\alpha_{sc}(M = 1, \lambda = -10, P = 0.6)(= 4.5473) < \alpha < \alpha_e(M = 1, P = 0.6)(= 4.6875)$. In the case of negative coupling $\lambda < 0$, we find a non-monotonically numerical solution for the scalar field. At large radial coordinates, it exhibits monotonically increasing behavior and tends to approach a positive constant at infinity. This implies that at infinity, the asymptotic condition for the scalar field shown in (34) should satisfy $d_1 < 0$, which is opposite to the case of $d_1 > 0$ in GB^+ scalarization with $\alpha = 0$. Therefore, the shooting conditions for finding numerical solutions are different. In this case, it is unable to find a numerical solution with $\psi_\infty = 0$ because under such a circumstance, the scalar $\psi(r)$ typically approaches a positive value at infinity.

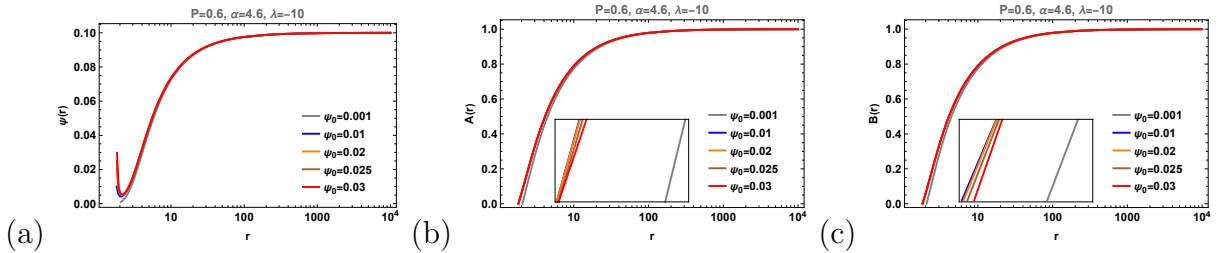


Figure 7: Scalarized cqOS black holes obtained from GB^- scalarization with $P = 0.6$, $\alpha = 4.6$, $\lambda = -10$. (a) Scalar $\psi(r)$ with $\psi_\infty = 0.1$. (b) Metric function $A(r)$. (c) Metric function $B(r)$.

Taking into account this special situation, we may choose $\psi_\infty = 0.1$ and $A(\infty) = B(\infty)$ as the shooting conditions to obtain numerical solutions. Here, ψ_0 is regarded as a free parameter that can be adjusted. However, across various coupling scenarios, all numerical solutions we can find indicate that the scalar constant ψ_0 cannot grow very large, implying that the constant scalar ψ_0 possessed by scalarized cqOS black holes is quite small.

For a choice of $\lambda = -10$, the scalar profile $\psi(r)$ and two metric functions $A(r)$ and $B(r)$ with different ψ_0 are shown in Fig. 7. An interesting observation is that although the scalar field increases monotonically at large radial coordinates, it exhibits nontrivial behavior in the near-horizon region. When $\psi_0 = 0.001$ is small, the scalar shows a monotonic growth trend. However, when ψ_0 is large, it decreases monotonically until reaching a local minimum and it starts to increase monotonically. It suggests strongly that the negative coupling in this model can cause the scalar to exhibit a decaying trend in the near-horizon region as well as a monotonically increasing trend in the far-region [29]. This is sharply compared to the decreasing behavior of scalar for GB^+ scalarization in Fig. 6.

Two metric functions $A(r)$ and $B(r)$ satisfy the conditions for the existence of a black hole. It approaches zero at the event horizon, then increases monotonically until it tends toward 1 at infinity. A notable feature is observed that when the constant scalar is small ($\psi_0 = 0.001$), the position of the event horizon is relatively large. As ψ_0 increases, however, the location of horizon rapidly decreases before slowly moving outward again. To clarify this behavior more explicitly, we plot the relation between the horizon radius r_+ and the scalar constant ψ_0 , as shown in Fig. 8. One can see that when the nontrivial scalar field first emerges, the black hole horizon radius decreases rapidly as ψ_0 increases. This decrease gradually becomes less pronounced as the coupling strength increases. However, as the scalar

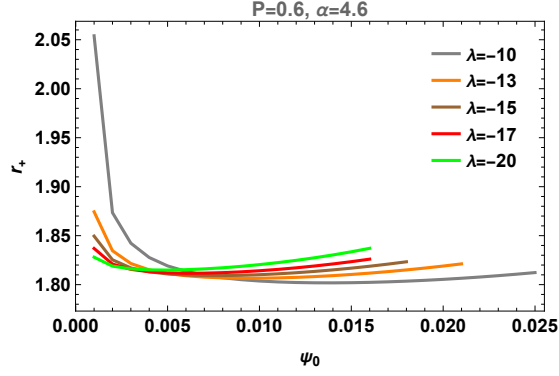


Figure 8: Horizon radius r_+ as a function of scalar constant ψ_0 .

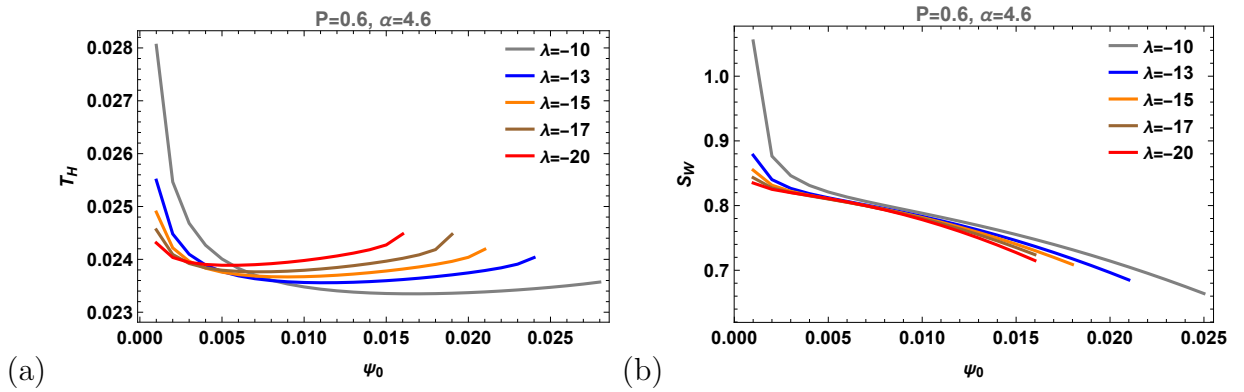


Figure 9: (a) Hawking temperature T_H and (b) Wald entropy S_W as functions of the constant scalar ψ_0 for different coupling constants ($\lambda = -10 \sim -20$).

constant continues to grow, we observe that the horizon radius begins to increase slowly. In contrast to the initial stage, the magnitude of this increase becomes more significant with increasing coupling strength.

This nonmonotonic relation directly influences the behavior of the thermodynamic quantities. So we further observe how the temperature and entropy behave according to the constant scalar ψ_0 and coupling constant λ . The Hawking temperature is defined as

$$T_H(r_+) = \frac{1}{4\pi} \sqrt{A'(r_+)B'(r_+)}. \quad (35)$$

Due to the GB term, the black hole entropy no longer follows the area-law. Instead, we compute the Wald entropy as

$$S_W = \frac{a_H(r_+)}{4} + 4\pi f(\psi_0), \quad (36)$$

where $a_H(r_+) = 4\pi r_+^2$ denotes the horizon area.

We wish to investigate the numerical solutions under different coupling constants. Fig. 9 illustrates the Hawking temperature and Wald entropy as functions of constant scalar ψ_0 . As shown in the figure, the functional behavior of the temperature is qualitatively similar to that of the horizon radius. As the scalar constant increases, the temperature first decreases rapidly and then grows slowly. An increase in the coupling strength suppresses the initial decrease but significantly enhances the subsequent rise in temperature. The Wald entropy, however, exhibits a different trend. This is because the negative contribution from the second term in Eq. (36) dominates over the first term.

It is worth noting that this is not the first time to observe the increasing behavior of a nontrivial scalar configuration. In Refs. [30, 31], hairy black-hole solutions arising from nonminimal coupling were found in which the scalar field develops a nonzero scalar constant near the horizon and approaches a constant value at spatial infinity. As the horizon value of the scalar field ψ_0 increases and eventually approaches the asymptotic value ψ_∞ , the scalar configuration becomes trivial, and the solution smoothly reduces to the vacuum black hole solution. By contrast, the hairy black holes found in the present work exhibit a more intricate structure. In the early stage, when ψ_0 is small, the horizon radius decreases rapidly, and the curves corresponding to different coupling strengths tend to approach a common curve. However, as ψ_0 continues to increase, Fig. 7(a) shows that the scalar field departs from the monotonic behavior as in Refs. [30, 31]. Instead, near the horizon the scalar field develops a nonmonotonic profile, first decreasing and then increasing. Consequently, the increase of ψ_0 no longer indicates that the configuration approaches the vacuum solution, as in Refs. [30, 31]; rather, it signals a further departure from the earlier monotonic behavior. Therefore, the hairy solutions obtained here cannot smoothly and continuously reduce to the vacuum black hole solution. When the coupling strength approaches zero, increasing ψ_0 may still show a tendency toward such a limit. However, as indicated by Fig. 5, this tendency is prevented once the coupling reaches its critical value.

5 Stability analysis for scalarized charged black hole

Before we proceed, it was shown for GB^+ scalarization that for an exponential coupling of $(1 - e^{-6\phi^2})/12$, its fundamental branch of scalarized black holes is stable against the radial

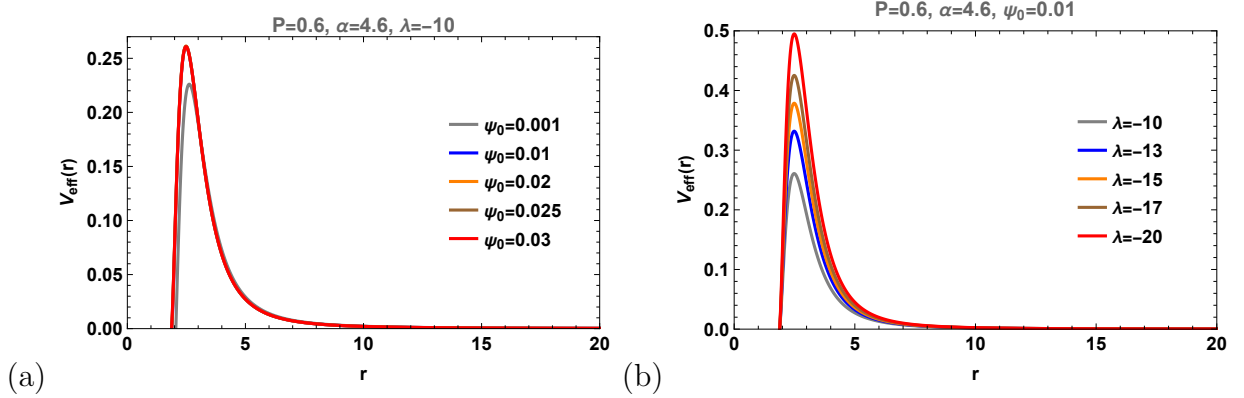


Figure 10: Radial profiles of effective potential under scalar perturbation for different (a) scalar constant ψ_0 and (b) coupling constants λ

perturbation [4, 5], while the fundamental branch of scalarized black holes is unstable against the radial perturbation for a quadratic coupling of ϕ^2 [32]. The latter branch is unstable because its width is short and it terminates at some nonzero mass due to violation of the regularity condition for r_+ . Hence, we are very curious to study the stability of scalarized black holes in the whole single branch obtained from GB^- scalarization with the quadratic coupling $f(\phi) = 2\lambda\phi^2$.

For this purpose, let us consider a linear perturbation of the scalar field around the background as $\phi = \psi(r) + \epsilon \frac{\delta\phi(r)}{r} e^{-i\omega t}$. Then, the perturbation equation takes the form

$$\frac{d^2\delta\phi(r)}{dr_*^2} + (\omega^2 - V_{\text{eff}}(r)) \delta\phi(r) = 0, \quad (37)$$

where the effective potential is given by

$$V_{\text{eff}}(r) = \frac{1}{2r^2 A(r)} \left[A(r) \left(r A(r)^2 B'(r) + 4\lambda(B(r) - 1)B(r)A'(r)^2 \right. \right. \\ \left. \left. + A'(r)[4\lambda(1 - 3B(r))B'(r) + rB(r)] - 8\lambda(B(r) - 1)B(r)A''(r) \right) \right], \quad (38)$$

with the tortoise coordinate r_* defined by $dr_* = \frac{dr}{\sqrt{A(r)B(r)}}$.

Fig. 10 displays the radial profiles of effective potential for the s -mode ($\ell = 0$) scalar perturbations under different values of ψ_0 and the coupling constant λ . As shown in this figure, the effective potential outside the event horizon exhibits a single-barrier structure without any negative regions. Moreover, the height of the potential barrier increases as either ψ_0 or the coupling constant λ becomes larger.

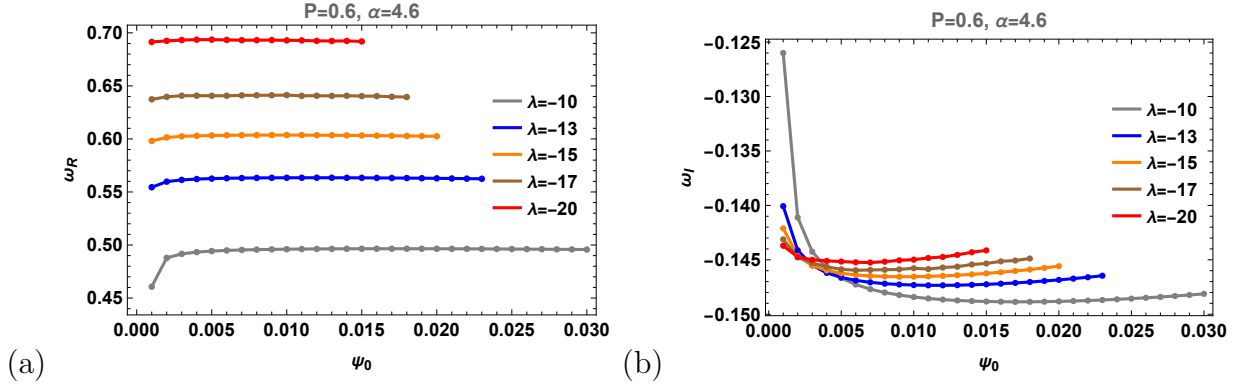


Figure 11: QNMs frequency. (a) real part ω_R and (b) imaginary part ω_I as the function of scalar constant ψ_0 for different coupling constants λ .

Any single-barrier potential typically predicts stability of the scalarized cQOS-black holes solution under scalar perturbations. To further substantiate this conclusion, we have to compute the quasinormal modes (QNMs) frequency. By imposing purely ingoing boundary condition at the horizon and purely outgoing boundary condition at spatial infinity, the QNMs frequency of $\omega = \omega_R + i\omega_I$ for different parameter choices can be obtained when adopting the pseudo-spectral method [33]. The corresponding results are presented in Fig. 11. We observe that when ψ_0 first becomes nonzero, both ω_R and ω_I exhibit pronounced variations: the real part increases rapidly, while the imaginary part decreases significantly. As ψ_0 increases further, ω_R continues to grow, but at a more moderate rate. In contrast, ω_I , after an initial rapid decrease, transitions to a slow increase at larger values of ψ_0 . An increase in the coupling constant substantially enhances the real part of the QNM frequency. The behavior of ω_I is more intricate: for small ψ_0 , increasing coupling constant tends to reduce the imaginary part, whereas for large ψ_0 , it leads to an increase.

Consequently, since ω_I remains negative for negative coupling constant λ throughout the parameter space considered, we confirm that the scalarized black hole solutions from GB^- scalarization are stable under scalar perturbations. In appendix A, we have plotted relevant physical quantities $(T_H, S_W, \omega_R, \omega_I)$ as functions of the horizon radius r_+ to get more comprehensive pictures. Fig. 13 confirms that the scalarized black hole solutions from GB^- scalarization are stable under scalar perturbations.

6 Discussions

We have investigated GB^- scalarization of cqOS-black holes obtained from the EGBS-NED theory. An important feature of these black holes is that they are described by mass M and action parameter α with a fixed magnetic charge P . This means that the magnetic charge P plays a subsidiary role in studying cqOS-black holes, contrasting with action parameter α .

We have studied thermodynamics of cqOS-black holes to obtain peculiar points of extremal point (α_e), Davies points (α_D, M_D), remnant point (M_{rem}), and allowed regions for the mass ($M \in [M_{\text{rem}}, \infty]$) and the action parameter ($\alpha \in [0, \alpha_e]$). Thermodynamic study was done by finding thermodynamic quantities, checking the first-law thermodynamics and the Smarr formula, and recognizing a phase transition at Davies points in the heat capacity.

Introducing $f(\phi) = 2\lambda\phi^2$ scalar coupling to GB term, we found onset of GB^- scalarization with critical onset parameters (α_c, M_c), implying that the single branch of scalarized cqOS-black holes exists. It is worth noting that the allowed unstable regions are narrow as $\alpha_{th}(M = 1, P = 0.6, \lambda) \in [\alpha_c, \alpha_e]$ and $M_{th}(\alpha = 1, P = 0.6, \lambda) \in [M_{\text{rem}}, M_c]$ for GB^- scalarization. To this model, we did not find any close connection between thermodynamics and onset of GB^- scalarization because the Davies curve obtained from heat capacity has nothing to do with the critical onset curve. This reflects that the nature of the present model is considered as charged quantum Oppenheimer-Snyder model [24], but not quantum Oppenheimer-Snyder model [19].

We have obtained all scalarized cqOS-black holes through GB^\pm scalarizations by solving Eqs.(2) and (6) numerically. In the case $\alpha = 0$ and $\lambda > 0$, which corresponds to GB^+ scalarization, our model reduces to the standard ESGB scenario for the Schwarzschild black hole. In contrast, for GB^- case with $\alpha \neq 0$ and $\lambda < 0$, a single branch of scalarized solutions is found in a narrow parameter space. It is worth noting that the scalar field displays nonmonotonic behavior near the horizon and approaches to a finite constant at infinity, indicating a qualitatively different scalarization driven by negative coupling. From a thermodynamic perspective, both Hawking temperature and Wald entropy exhibit nontrivial dependence on the scalar constant ψ_0 , reflecting the nonmonotonic variation of the horizon radius.

Finally, we have examined linear stability of scalarized cqOS-black holes under scalar perturbations. We found that the effective potential possesses a single-barrier structure,

and all QNM frequencies satisfy $\omega_I < 0$ throughout the parameter space considered. This demonstrates clearly that the scalarized cqOS-black holes obtained from GB^- scalarization are linearly stable against scalar perturbations, completing a consistent picture of their existence, thermodynamic behavior, and dynamical stability. This is compared to the case that the fundamental branch of scalarized black holes obtained from GB^+ scalarization is unstable against the radial perturbation for a quadratic coupling of ϕ^2 in the EGBS theory [32].

7 Acknowledgments

W.K. and Y.S.M. are supported by the National Research Foundation of Korea (NRF) grant funded by the Korea government (MSIT) (RS-2022-NR069013). H.G. is supported by the Institute for Basic Science (Grant No. IBS-R018-Y1).

A Physical quantities as function of horizon radius r_+

In the text, we plotted all figures as function the scalar at the horizon ($\psi_0 = \psi(r_+)$). Making use of the numerical connection between r_+ and ψ_0 , we have temperature and entropy expressed in terms of r_+ as are shown in Fig. 12. According to Fig. 8, as the scalar constant ψ_0 increases, the horizon radius first decreases rapidly and then increases slowly. Consequently, as shown in Fig. 12, the Hawking temperature exhibits two distinct regimes that are positively correlated with the horizon radius r_+ . In the early stage, the Hawking temperature decreases rapidly as r_+ becomes smaller. In the later stage, as r_+ gradually increases, the temperature grows monotonically. The behavior of the Wald entropy is different. In the early stage, it shows a positive correlation with r_+ , whereas in the later stage it becomes negatively correlated with r_+ .

For the QNM frequencies, the imaginary part ω_I displays a qualitatively similar behavior to the Hawking temperature: it remains positively correlated with r_+ in both the early and late stages. It is also worth noting that, in the plot of the real part, each curve exhibits a turning point, while the imaginary part shows increasingly pronounced oscillations as the coupling strength becomes larger. However, it confirms that these of all negative ω_I shows

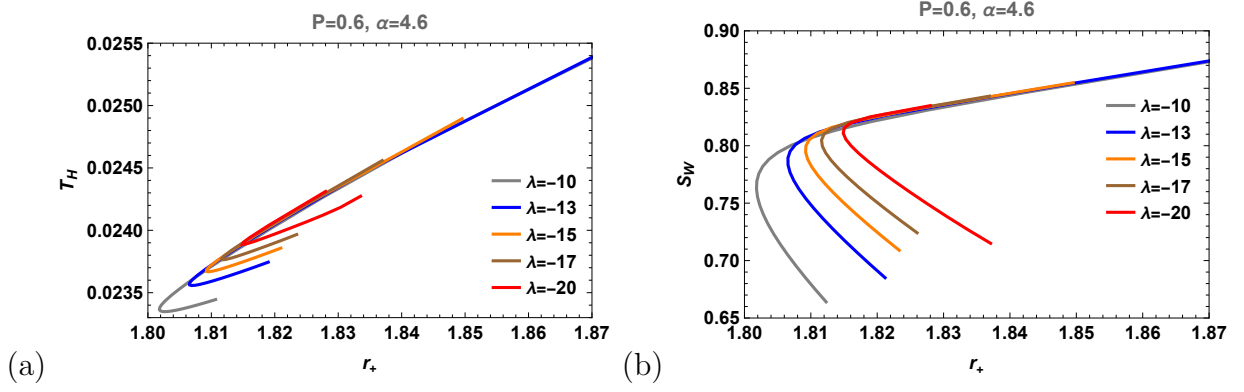


Figure 12: (a) Hawking temperature T_H and (b) Wald entropy S_W as functions of the horizon radius r_+ for different coupling constants ($\lambda = -10 \sim -20$).

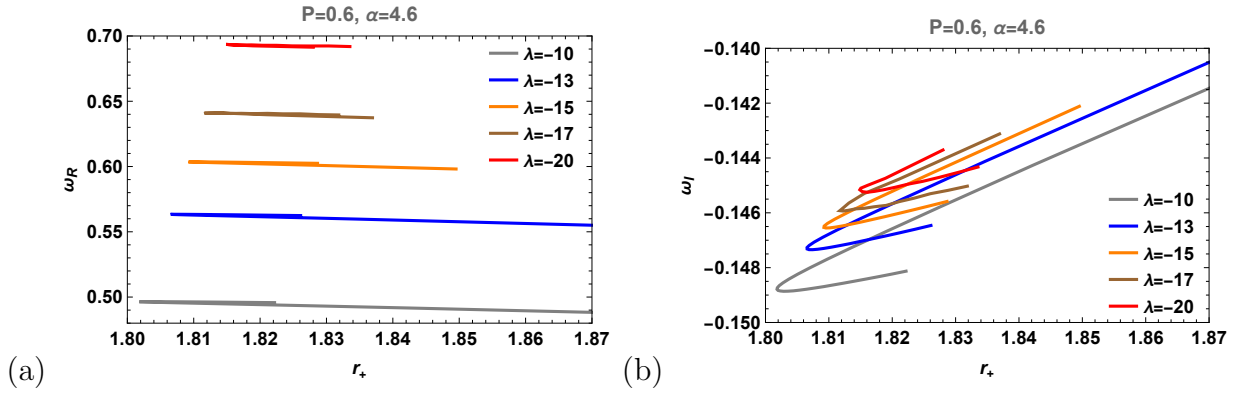


Figure 13: QNMs frequency. (a) real part ω_R and (b) imaginary part ω_I as the function of horizon radius r_+ for different coupling constants λ .

still the stability of scalarized cqOS black holes obtained from GB^- scalarization.

References

- [1] B. Carter, Phys. Rev. Lett. **26** (1971), 331-333 doi:10.1103/PhysRevLett.26.331
- [2] R. Ruffini and J. A. Wheeler, Phys. Today **24** (1971) no.1, 30 doi:10.1063/1.3022513
- [3] C. A. R. Herdeiro and E. Radu, Int. J. Mod. Phys. D **24** (2015) no.09, 1542014 doi:10.1142/S0218271815420146 [arXiv:1504.08209 [gr-qc]].
- [4] D. D. Doneva and S. S. Yazadjiev, Phys. Rev. Lett. **120** (2018) no.13, 131103 doi:10.1103/PhysRevLett.120.131103 [arXiv:1711.01187 [gr-qc]].
- [5] H. O. Silva, J. Sakstein, L. Gualtieri, T. P. Sotiriou and E. Berti, Phys. Rev. Lett. **120** (2018) no.13, 131104 doi:10.1103/PhysRevLett.120.131104 [arXiv:1711.02080 [gr-qc]].
- [6] G. Antoniou, A. Bakopoulos and P. Kanti, Phys. Rev. Lett. **120** (2018) no.13, 131102 doi:10.1103/PhysRevLett.120.131102 [arXiv:1711.03390 [hep-th]].
- [7] C. A. R. Herdeiro, E. Radu, N. Sanchis-Gual and J. A. Font, Phys. Rev. Lett. **121** (2018) no.10, 101102 doi:10.1103/PhysRevLett.121.101102 [arXiv:1806.05190 [gr-qc]].
- [8] Y. S. Myung and D. C. Zou, Eur. Phys. J. C **79** (2019) no.3, 273 doi:10.1140/epjc/s10052-019-6792-6 [arXiv:1808.02609 [gr-qc]].
- [9] Y. S. Myung and D. C. Zou, Phys. Lett. B **790** (2019), 400-407 doi:10.1016/j.physletb.2019.01.046 [arXiv:1812.03604 [gr-qc]].
- [10] P. Cunha, V.P., C. A. R. Herdeiro and E. Radu, Phys. Rev. Lett. **123** (2019) no.1, 011101 doi:10.1103/PhysRevLett.123.011101 [arXiv:1904.09997 [gr-qc]].
- [11] L. G. Collodel, B. Kleihaus, J. Kunz and E. Berti, Class. Quant. Grav. **37** (2020) no.7, 075018 doi:10.1088/1361-6382/ab74f9 [arXiv:1912.05382 [gr-qc]].
- [12] A. Dima, E. Barausse, N. Franchini and T. P. Sotiriou, Phys. Rev. Lett. **125** (2020) no.23, 231101 doi:10.1103/PhysRevLett.125.231101 [arXiv:2006.03095 [gr-qc]].
- [13] S. Hod, Phys. Rev. D **102** (2020) no.8, 084060 doi:10.1103/PhysRevD.102.084060 [arXiv:2006.09399 [gr-qc]].

- [14] S. J. Zhang, B. Wang, A. Wang and J. F. Saavedra, *Phys. Rev. D* **102** (2020) no.12, 124056 doi:10.1103/PhysRevD.102.124056 [arXiv:2010.05092 [gr-qc]].
- [15] D. D. Doneva, L. G. Collodel, C. J. Krüger and S. S. Yazadjiev, *Phys. Rev. D* **102** (2020) no.10, 104027 doi:10.1103/PhysRevD.102.104027 [arXiv:2008.07391 [gr-qc]].
- [16] M. Y. Lai, Y. S. Myung, R. H. Yue and D. C. Zou, *Phys. Rev. D* **106** (2022) no.4, 044045 doi:10.1103/PhysRevD.106.044045 [arXiv:2206.11587 [gr-qc]].
- [17] M. Y. Lai, Y. S. Myung, R. H. Yue and D. C. Zou, *Phys. Rev. D* **106** (2022) no.8, 084043 doi:10.1103/PhysRevD.106.084043 [arXiv:2208.11849 [gr-qc]].
- [18] Z. Belkhadria and S. Mignemi, *Phys. Rev. D* **112** (2025) no.4, 044015 doi:10.1103/ln23-nhpn [arXiv:2506.12137 [gr-qc]].
- [19] J. Lewandowski, Y. Ma, J. Yang and C. Zhang, *Phys. Rev. Lett.* **130** (2023) no.10, 101501 doi:10.1103/PhysRevLett.130.101501 [arXiv:2210.02253 [gr-qc]].
- [20] S. H. Dong, F. Hosseinifar, F. Studnička and H. Hassanabadi, *Phys. Lett. B* **860** (2025), 139182 doi:10.1016/j.physletb.2024.139182
- [21] J. P. Ye, Z. Q. He, A. X. Zhou, Z. Y. Huang and J. H. Huang, *Phys. Lett. B* **851** (2024), 138566 doi:10.1016/j.physletb.2024.138566 [arXiv:2312.17724 [gr-qc]].
- [22] L. Chen and S. Jiang, *Phys. Lett. B* **866** (2025), 139522 doi:10.1016/j.physletb.2025.139522
- [23] Y. S. Myung, *Eur. Phys. J. C* **85** (2025) no.7, 745 doi:10.1140/epjc/s10052-025-14472-8 [arXiv:2505.19450 [gr-qc]].
- [24] S. H. Mazharimousavi, *Eur. Phys. J. C* **85** (2025) no.6, 667 doi:10.1140/epjc/s10052-025-14410-8 [arXiv:2502.10457 [gr-qc]].
- [25] M. Hassaine and C. Martinez, *Class. Quant. Grav.* **25** (2008), 195023 doi:10.1088/0264-9381/25/19/195023 [arXiv:0803.2946 [hep-th]].
- [26] G. Dotti and R. J. Gleiser, *Class. Quant. Grav.* **22** (2005), L1 doi:10.1088/0264-9381/22/1/L01 [arXiv:gr-qc/0409005 [gr-qc]].

- [27] D. D. Doneva, S. Kiorpelidi, P. G. Nedkova, E. Papantonopoulos and S. S. Yazadjiev, *Phys. Rev. D* **98** (2018) no.10, 104056 doi:10.1103/PhysRevD.98.104056 [arXiv:1809.00844 [gr-qc]].
- [28] Y. S. Myung and D. C. Zou, *Phys. Rev. D* **98** (2018) no.2, 024030 doi:10.1103/PhysRevD.98.024030 [arXiv:1805.05023 [gr-qc]].
- [29] Y. Brihaye and B. Hartmann, *Phys. Lett. B* **792**, 244-250 (2019) doi:10.1016/j.physletb.2019.03.043 [arXiv:1902.05760 [gr-qc]].
- [30] H. Guo, W. L. Qian and B. Wang, *Phys. Rev. D* **112** (2025) no.8, 8 doi:10.1103/861k-193h [arXiv:2506.02445 [gr-qc]].
- [31] H. Guo, H. Liu and Y. S. Myung, *Eur. Phys. J. C* **86** (2026) no.2, 204 doi:10.1140/epjc/s10052-026-15407-7 [arXiv:2512.22433 [gr-qc]].
- [32] J. L. Blázquez-Salcedo, D. D. Doneva, J. Kunz and S. S. Yazadjiev, *Phys. Rev. D* **98**, no.8, 084011 (2018) doi:10.1103/PhysRevD.98.084011 [arXiv:1805.05755 [gr-qc]].
- [33] A. Jansen, *Eur. Phys. J. Plus* **132** (2017) no.12, 546 doi:10.1140/epjp/i2017-11825-9 [arXiv:1709.09178 [gr-qc]].